IEEE Access
Multidisciplinary | Rapid Review | Open Access Journal

Received June 6, 2017, accepted June 24, 2017, date of publication June 29, 2017, date of current version August 14, 2017.

Digital Object Identifier 10.1109/ACCESS.2017.2721459

Robust Adaptive Backstepping Sliding Mode Control for Six-Phase Permanent Magnet Synchronous Motor Using Recurrent Wavelet Fuzzy Neural Network

LIU SHENG, GUO XIAOJIE, AND ZHANG LANYONG, (Member, IEEE)
Department of Automation, Harbin Engineering University, Harbin 150001, China

Corresponding author: Guo Xiaojie (lucky_gxj_0372@163.com)

This work was supported in part by the National Natural Science Foundation of China Subsidization Project under Grant 51579047, in part by the Doctoral Scientific Research Foundation of Heilongjiang under Grant LBH-Q14040, in part by the National Defense Technology Fundamental Research Funds under Grant JSHS2015604C002, and in part by the Open Project Program of State Key Laboratory of Millimeter Waves under Grant K201707.

ABSTRACT A robust adaptive backstepping sliding mode control (ABSMC) with recurrent wavelet fuzzy neural network (RWFNN) is proposed for the speed regulation of a six-phase permanent magnet synchronous motor (PMSM) demonstrating parameter perturbations and load disturbances. First, a motor drive system model with lumped uncertainty is developed. Then, a nonlinear robust speed controller using ABSMC and H_∞ theory is presented. In this technique, ABSMC is employed to guarantee the speed tracking and parameter perturbation suppression; meanwhile, nonlinear H_∞ is utilized to minimize the influence of dynamic load disturbances on its tracking output. In addition, an uncertainty observer based on the RWFNN is designed to estimate the unknown and improve the robustness of motor drive system further. Ultimately, simulations and AppSIM simulator-based experimental results both indicate that the proposed control scheme can perfectly compensate the parameter perturbations and load disturbances while maintaining speed tracking precision.

INDEX TERMS Permanent magnet synchronous motor (PMSM), adaptive backstepping sliding mode (ABSM), nonlinear robust control, recurrent wavelet fuzzy neural network (RWFNN), uncertainty observer.

I. INTRODUCTION

Recently, permanent magnet synchronous motors (PMSMs) have been extensively applied in many fields such as numerically-controlled machine tools, aerospace, ship electric propulsion for its advantages like compact structure, simple control, high power density [1], [2]. Compared with traditional three-phase motors, multiphase PMSMs have incomparable strengths, for instance, high output power with low voltage, high system reliability, small torque ripple etc. [3], [4]. Therefore, it is of great theoretical significance and practical value to study the speed control system of a six-phase dual Y shift 30° PMSM.

The classical proportional integral (PI) control technique is universally employed in the current six-phase PMSM system due to its high reliability and simple implementation [5]. However, linear PI controller cannot eliminate its dependence on the plant model and parameters; especially, the internal parameter perturbations and external disturbances (called lumped uncertainty), which occur in the applications of six-phase PMSM system. It is difficult to meet the requirement of high-performance speed control needed for the nonlinear drive system. Therefore, advanced nonlinear control methods such as robust theory [6]–[8], predictive control [9], [10], sliding mode control [11], [12], backstepping technique [13], [14] and intelligent algorithm [15]–[17] have been introduced into the motors control system.

Backstepping is a systemic and recursive design method for nonlinear feedback control. As for the uncertain PMSM drive system, the adaptive backstepping control, that combines backstepping technique and adaptive theory, is generally adopted, as it can reduce the design burden on the stability control and parameter estimation [18]–[21]. Sliding mode variable structure control is highly robust and has high control accuracy for internal parameter perturbations and external disturbances [22], [23]; however, it has limitations of inherent chattering and the need to meet the matching

conditions of disturbances. In order to improve the robustness of adaptive backstepping strategy and overcome the disturbance-matching limitation of sliding mode control, the adaptive backstepping sliding mode control (ABSMC) algorithm has been developed and utilized in the motors control system [24]–[26].

The wavelet fuzzy neural network (WFNN), a combination of the merits of fuzzy neural network for learning from process and wavelet decomposition for identification of dynamic system, has been proved to be better than the other neural networks in that the structure can provide more potential to enrich the mapping relationship between inputs and outputs [13], [27]. Since most of the practical applications are dynamic, the recurrent structure has been added into WFNN to enhance its ability of dynamic mapping and temporal information storage [28], [29]. As a novel universal approximator, recurrent wavelet fuzzy neural network (RWFNN) can estimate the parameter perturbations and unknown disturbances to realize real-time compensation of lumped uncertainty in the PMSM drive system [3], [15], [16].

Recently, many researchers have been investigating the modeling methods of multiphase motors and the ABSMC techniques for three-phase motors [30]–[37]. However, in the forementioned six-phase PMSM system design for the speed loop, usually a first-order model is used to approximately describe the relationship between the reference q axis currents and the speed output, by neglecting the dynamic responses of the q axis current loops, thus degrading the closed-loop control performance [3], [11], [38], [39]. Further, in the presence of unknown load disturbances, with wide range of changes and fast variations, the characteristic of ABSMC-based methods will be affected by assuming load torque as a slow-varying parameter. Additionally, since six-phase motors have problems in double controlled quantity and coordinated allocation of stator currents on the d-q axis, it is difficult to directly promote control strategies for three-phase motors to the six-phase PMSM regulation system.

The contribution of this study is to develop an AppSIM simulator-based nonlinear robust ABSM controller with RWFNN uncertainty observer for the speed regulation of a six-phase PMSM drive system under the lumped uncertainty. In the paper, a mathematical model in the synchronous rotating reference frame is introduced first, which considers the parameter perturbations and load disturbances. Then, with the implementation of field-oriented control, a robust ABSM controller, that takes the integration of the speed loop and current loops with load disturbance rejection into account, is presented to compensate the uncertainty while maintaining speed tracking. In the proposed technique, ABSMC is employed to guarantee the speed tracking and parameter perturbation suppression. Meanwhile, nonlinear H_∞ is utilized to minimize the influence of dynamic load disturbances on its tracking output. Furthermore, to improve the anti-interference robustness and parameter insensitivity, a RWFNN observer is proposed for the real-time uncertainty compensation, and the online learning process of network parameters is designed. The anti-interference robustness is defined as the effect of lumped uncertainty on the speed response for the PMSM drive system. Likewise, the parameter insensitivity implies avoiding parameter tuning problems arising during the estimation of uncertain information. In addition, the proposed control scheme is implemented in an AppSIM real-time simulator and the validity of the proposed control algorithm is verified by the simulations and experimental results.

This paper is organized as follows. Section II introduces the mathematical model of a six-phase PMSM system suitable for controller design. Section III presents the design details of nonlinear robust speed controller and stability proof using the Lyapunov stability criterion. The effectiveness of the control scheme is verified through simulations and experimental results in Section IV and V, respectively. Related conclusions are given in Section VI.

II. MODEL OF SIX-PHASE PMSM DRIVE SYSTEM

The mathematical model for a six-phase dual Y shift 30° surface-mounted PMSM in the synchronous rotating d-q coordinates mainly consists of the stator voltage equation, the stator linkage equation, the electromagnetic torque equation, and the mechanical motion equation. The stator voltage equation can be expressed as

$$\begin{cases} u_{d1} = R_s i_{d1} + \dfrac{d\psi_{d1}}{dt} - n_p\omega\psi_{q1} \\ u_{q1} = R_s i_{q1} + \dfrac{d\psi_{q1}}{dt} + n_p\omega\psi_{d1} \\ u_{d2} = R_s i_{d2} + \dfrac{d\psi_{d2}}{dt} - n_p\omega\psi_{q2} \\ u_{q2} = R_s i_{q2} + \dfrac{d\psi_{q2}}{dt} + n_p\omega\psi_{d2} \end{cases} \tag{1}$$

The stator linkage equation is shown as

$$\begin{cases} \psi_{d1} = L_d i_{d1} + L_{md} i_{d2} + \psi_f \\ \psi_{q1} = L_q i_{q1} + L_{mq} i_{q2} \\ \psi_{d2} = L_{md} i_{d1} + L_d i_{d2} + \psi_f \\ \psi_{q2} = L_{mq} i_{q1} + L_q i_{q2} \end{cases} \tag{2}$$

The electromagnetic torque equation can be written as

$$T_e = \frac{3n_p}{2}\left(\psi_{d1} i_{q1} + \psi_{d2} i_{q2} - \psi_{q1} i_{d1} - \psi_{q2} i_{d2}\right) \tag{3}$$

The mechanical motion equation is given by

$$T_e - T_L - B_\omega\omega = J\frac{d\omega}{dt} \tag{4}$$

where u_{dn} and u_{qn} refer to the d-q axis voltages of the nth set of stator windings and n=1 or 2; i_{dn} and i_{qn} are the d-q axis currents of the nth set of stator windings; ψ_{dn} and ψ_{qn} are the d-q axis flux linkages of the nth set of stator windings; L_d and L_q refer to the d-q axis inductances ($L_d = L_q = L$); L_{md} and L_{mq} are the d-q axis mutual inductances of the two sets of stator windings ($L_{md} = L_{mq} = L_m$); R_s is the stator resistance; n_p is the number of pole pairs; ψ_f is the flux linkage of permanent magnet; T_e and T_L are the electromagnetic torque and load torque, respectively; B_ω is

the friction coefficient; J is the moment of inertia; ω is the rotor angular velocity.

For the speed controller design, the rotor angular velocity and the stator currents are chosen as state variables. According to equations (1) - (4), the state space model of the six-phase PMSM drive system can be written as the following equation.

$$\begin{cases} \dfrac{d\omega}{dt} = \dfrac{3n_p}{2J}\psi_f(i_{q1}+i_{q2}) - \dfrac{T_L}{J} - \dfrac{B_\omega}{J}\omega \\ \dfrac{di_{d1}}{dt} = \gamma_1 u_{d1} - \gamma_2 u_{d2} - \gamma_1 R_s i_{d1} + \gamma_2 R_s i_{d2} + n_p\omega i_{q1} \\ \dfrac{di_{q1}}{dt} = \gamma_1 u_{q1} - \gamma_2 u_{q2} - \gamma_1 R_s i_{q1} + \gamma_2 R_s i_{q2} - n_p\omega i_{d1} \\ \qquad - \gamma_3 n_p\omega\psi_f \\ \dfrac{di_{d2}}{dt} = \gamma_1 u_{d2} - \gamma_2 u_{d1} - \gamma_1 R_s i_{d2} + \gamma_2 R_s i_{d1} + n_p\omega i_{q2} \\ \dfrac{di_{q2}}{dt} = \gamma_1 u_{q2} - \gamma_2 u_{q1} - \gamma_1 R_s i_{q2} + \gamma_2 R_s i_{q1} - n_p\omega i_{d2} \\ \qquad - \gamma_3 n_p\omega\psi_f \end{cases} \tag{5}$$

where $\gamma_1 = \frac{L}{L^2-L_m^2}$, $\gamma_2 = \frac{L_m}{L^2-L_m^2}$, $\gamma_3 = \frac{1}{L+L_m}$.

Due to various parameter perturbations and load disturbances in the complicated environments of the six-phase PMSM drive, one redefines the state equation in the following matrix form to realize online real-time estimation of system uncertainty.

$$\frac{dx}{dt} = f_N(x) + \Delta f(x) + g(x)u \tag{6}$$

where

$$x = [\omega \quad i_{d1} \quad i_{q1} \quad i_{d2} \quad i_{q2}]^T,$$

$$u = [u_{d1} \quad u_{q1} \quad u_{d2} \quad u_{q2}]^T, \quad d = \frac{T_L}{J},$$

$$f_N(x) = \begin{bmatrix} f_{N1} \\ f_{N2} \\ f_{N3} \\ f_{N4} \\ f_{N5} \end{bmatrix} = \begin{bmatrix} a_{1N}(i_{q1}+i_{q2}) - a_{2N}\omega \\ -a_{5N}i_{d1} + a_{6N}i_{d2} + n_p\omega i_{q1} \\ -a_{5N}i_{q1} + a_{6N}i_{q2} - n_p\omega i_{d1} - a_{7N}\omega \\ -a_{5N}i_{d2} + a_{6N}i_{d1} + n_p\omega i_{q2} \\ -a_{5N}i_{q2} + a_{6N}i_{q1} - n_p\omega i_{d2} - a_{7N}\omega \end{bmatrix},$$

$$g(x) = \begin{bmatrix} 0 & 0 & 0 & 0 \\ a_{3N} & 0 & -a_{4N} & 0 \\ 0 & a_{3N} & 0 & -a_{4N} \\ -a_{4N} & 0 & a_{3N} & 0 \\ 0 & -a_{4N} & 0 & a_{3N} \end{bmatrix},$$

$$\Delta f(x) = \begin{bmatrix} \Delta a_{1N}(i_{q1}+i_{q2}) - \Delta a_{2N}\omega - d \\ -\Delta a_{5N}i_{d1} + \Delta a_{6N}i_{d2} + \Delta a_{3N}u_{d1} - \Delta a_{4N}u_{d2} \\ -\Delta a_{5N}i_{q1} + \Delta a_{6N}i_{q2} - \Delta a_{7N}\omega + \Delta a_{3N}u_{q1} - \Delta a_{4N}u_{q2} \\ -\Delta a_{5N}i_{d2} + \Delta a_{6N}i_{d1} + \Delta a_{3N}u_{d2} - \Delta a_{4N}u_{d1} \\ -\Delta a_{5N}i_{q2} + \Delta a_{6N}i_{q1} - \Delta a_{7N}\omega + \Delta a_{3N}u_{q2} - \Delta a_{4N}u_{q1} \end{bmatrix},$$

$$a_1 = \frac{3n_p}{2J}\psi_f, a_2 = \frac{B_\omega}{J}, \ a_3 = \gamma_1, \ a_4 = \gamma_2,$$

$$a_5 = \gamma_1 R_s, a_6 = \gamma_2 R_s, \ a_7 = \gamma_3 n_p \psi_f,$$

$$a_i = a_{iN} + \Delta a_{iN}, \quad i = 1, \ldots\ldots 7.$$

In the above, the subscript "N" stands for the nominal value of the parameters and the symbol "Δ" represents the perturbation factor in the parameters.

The variable θ is introduced as

$$\theta = [\Delta a_{1N} \quad \Delta a_{2N} \quad \ldots \quad \Delta a_{7N}]^T$$

By substituting the expressions for $f_N(x)$, $g(x)$ and $\Delta f(x)$ into equation (6), the mathematical model of six-phase PMSM system, suitable for the robust ABSM controller design, is obtained as follows.

$$\begin{cases} \dfrac{d\omega}{dt} = f_{N1} + \theta^T\alpha_1 - d \\ \dfrac{di_{d1}}{dt} = f_{N2} + a_{3N}u_{d1} - a_{4N}u_{d2} + \theta^T\alpha_2 \\ \dfrac{di_{q1}}{dt} = f_{N3} + a_{3N}u_{q1} - a_{4N}u_{q2} + \theta^T\alpha_3 \\ \dfrac{di_{d2}}{dt} = f_{N4} + a_{3N}u_{d2} - a_{4N}u_{d1} + \theta^T\alpha_4 \\ \dfrac{di_{q2}}{dt} = f_{N5} + a_{3N}u_{q2} - a_{4N}u_{q1} + \theta^T\alpha_5 \end{cases} \tag{7}$$

where

$$\alpha = \begin{bmatrix} \alpha_1 \\ \alpha_2 \\ \alpha_3 \\ \alpha_4 \\ \alpha_5 \end{bmatrix}^T = \begin{bmatrix} i_{q1}+i_{q2} & -\omega & 0 & 0 & 0 & 0 & 0 \\ 0 & 0 & u_{d1} & -u_{d2} & -i_{d1} & i_{d2} & 0 \\ 0 & 0 & u_{q1} & -u_{q2} & -i_{q1} & i_{q2} & -\omega \\ 0 & 0 & u_{d2} & -u_{d1} & -i_{d2} & i_{d1} & 0 \\ 0 & 0 & u_{q2} & -u_{q1} & -i_{q2} & i_{q1} & -\omega \end{bmatrix}^T$$

III. DESIGN OF SPEED CONTROLLERS

A. DESIGN OF THE ROBUST ABSM CONTROLLER

The control objective of the six-phase PMSM speed regulation system is that the designed controller can guarantee the high performance of speed trajectory tracking and lumped uncertainty suppression. The proposed nonlinear robust speed controller using the ABSM method and H_∞ theory is presented and described step by step as follows.

Step 1: To design the speed controller, the speed tracking error and its time derivative along the solution trajectory of system (7) are defined as

$$\begin{cases} e_\omega = \omega - \omega^* \\ \dfrac{de_\omega}{dt} = f_{N1} + \theta^T\alpha_1 - d - \dfrac{d\omega^*}{dt} \end{cases} \tag{8}$$

where ω^* is the speed reference trajectory.

The first Lyapunov stability function is chosen as $V_1 = \frac{e_\omega^2}{2}$. Define the energy function $H_1 = \frac{dV_1}{dt} + \frac{1}{2}(\|e_\omega\|^2 - \gamma^2\|d\|^2)$,

thus

$$H_1 = e_\omega(f_{N1} + \theta^T\alpha_1 - d - \frac{d\omega^*}{dt}) + \frac{1}{2}(\|e_\omega\|^2 - \gamma^2\|d\|^2)$$
$$= -(k_\omega - \frac{1}{\gamma^2} - \frac{1}{2})e_\omega^2 + e_\omega[a_{1N}(i_{q1} + i_{q2}) - a_{2N}\omega + \theta^T\alpha_1 - \frac{d\omega^*}{dt} + k_\omega e_\omega] - (\frac{\gamma}{2}d + \frac{e_\omega}{\gamma})^2 - \frac{\gamma^2}{4}d^2 \quad (9)$$

where $k_\omega - 1/\gamma^2 - 1/2 > 0$ is a positive constant, and $\gamma > 0$ is the effect attenuation constant of load disturbances on tracking error in L_2 space.

Accordingly, the ideal pseudo-control inputs and tracking errors of stator currents on the q axis are adopted as

$$i_{q1}^* = i_{q2}^* = \frac{1}{2a_{1N}}(a_{2N}\omega - \hat\theta^T\alpha_1 + \frac{d\omega^*}{dt} - k_\omega e_\omega)$$
$$\begin{cases} e_{q1} = i_{q1} - i_{q1}^* \\ e_{q2} = i_{q2} - i_{q2}^* \end{cases} \quad (10)$$

where $\hat\theta$ refers to the estimated value of the uncertain parameter θ. Note that the estimation error $\tilde\theta = \hat\theta - \theta$, and then it follows

$$H_1 = -(k_\omega - \frac{1}{\gamma^2} - \frac{1}{2})e_\omega^2 + e_\omega[a_{1N}(e_{q1} + e_{q1}) - \tilde\theta^T\alpha_1] - (\frac{\gamma}{2}d + \frac{e_\omega}{\gamma})^2 - \frac{\gamma^2}{4}d^2 \quad (11)$$

Step 2: With the implementation of field-oriented control, the ideal pseudo-control inputs and tracking errors of stator currents on the d axis are adopted as

$$i_{d1}^* = i_{d2}^* = 0$$
$$\begin{cases} e_{d1} = i_{d1} - i_{d1}^* \\ e_{d2} = i_{d2} - i_{d2}^* \end{cases} \quad (12)$$

To ensure the speed tracking performance and uncertain disturbance rejection ability, the augmented Lyapunov function V_2 is selected as

$$V_2 = V_1 + \frac{1}{2}s_{d1}^2 + \frac{1}{2}s_{d2}^2 + \frac{1}{2}s_{q1}^2 + \frac{1}{2}s_{q2}^2 + \frac{1}{2}\tilde\theta^T P\tilde\theta \quad (13)$$

where P denotes a positive definite symmetric matrix. s_{d1}, s_{d2}, s_{q1}, and s_{q2} are the integral sliding surfaces corresponding with e_{d1}, e_{d2}, e_{q1}, and e_{q2} respectively, which are defined as follows.

$$\begin{cases} s_{d1} = e_{d1} + \lambda_d\int_0^t e_{d1}d\tau \\ s_{d2} = e_{d2} + \lambda_d\int_0^t e_{d2}d\tau \\ s_{q1} = e_{q1} + \lambda_q\int_0^t e_{q1}d\tau \\ s_{q2} = e_{q2} + \lambda_q\int_0^t e_{q2}d\tau \end{cases} \quad (14)$$

where λ_d, λ_q are the sliding surface gains.

Define the function $H_2 = \frac{dV_2}{dt} + \frac{1}{2}(\|e_\omega\|^2 - \gamma^2\|d\|^2)$ for the closed-loop system, and it holds that

$$H_2 = H_1 + s_{d1}\frac{ds_{d1}}{dt} + s_{d2}\frac{ds_{d2}}{dt} + s_{q1}\frac{ds_{q1}}{dt} + s_{q2}\frac{ds_{q2}}{dt} + \tilde\theta^T P\frac{d\tilde\theta}{dt}$$
$$= -(k_\omega - \frac{1}{\gamma^2} - \frac{1}{2})e_\omega^2 - k_d s_{d1}^2 - k_d s_{d2}^2 - k_q s_{q1}^2 - k_q s_{q2}^2 - k_\theta\tilde\theta^T\tilde\theta - (\frac{\gamma}{2}d + \frac{e_\omega}{\gamma})^2 - \frac{\gamma^2}{4}d^2 + a_{1N}e_\omega(e_{q1} + e_{q1}) + s_{d1}(f_{N2} + a_{3N}u_{d1} - a_{4N}u_{d2} + \hat\theta^T\alpha_2 + \lambda_d e_{d1} + k_d s_{d1}) + s_{d2}(f_{N4} + a_{3N}u_{d2} - a_{4N}u_{d1} + \hat\theta^T\alpha_4 + \lambda_d e_{d2} + k_d s_{d2}) + s_{q1}(f_{N3} + a_{3N}u_{q1} - a_{4N}u_{q2} + \hat\theta^T\alpha_3 - \frac{di_{q1}^*}{dt} + k_q s_{q1} + \lambda_q e_{q1}) + s_{q2}(f_{N5} + a_{3N}u_{q2} - a_{4N}u_{q1} + \hat\theta^T\alpha_5 - \frac{di_{q2}^*}{dt} + k_q s_{q2} + \lambda_q e_{q2}) + \tilde\theta^T \times (P\frac{d\tilde\theta}{dt} - e_\omega\alpha_1 - s_{d1}\alpha_2 - s_{d2}\alpha_4 - s_{q1}\alpha_3 - s_{q2}\alpha_5 + k_\theta\tilde\theta) \quad (15)$$

where k_d, k_q, and k_θ refer to positive constants remaining to be designed.

Thus, to guarantee the practical stability operation of six-phase PMSM closed-loop system, the nonlinear robust control law is designed as follows.

$$\begin{cases} u_{d1} = \frac{-1}{a_{3N}^2 - a_{4N}^2} \times \begin{bmatrix} a_{3N}f_{N2} + a_{4N}f_{N4} + \hat\theta^T(a_{3N}\alpha_2 + a_{4N}\alpha_4) \\ + \lambda_d(a_{3N}e_{d1} + a_{4N}e_{d2}) + k_d(a_{3N}s_{d1} + a_{4N}s_{d2}) \end{bmatrix} \\ u_{d2} = \frac{-1}{a_{3N}^2 - a_{4N}^2} \times \begin{bmatrix} a_{4N}f_{N2} + a_{3N}f_{N4} + \hat\theta^T(a_{4N}\alpha_2 + a_{3N}\alpha_4) \\ + \lambda_d(a_{4N}e_{d1} + a_{3N}e_{d2}) + k_d(a_{4N}s_{d1} + a_{3N}s_{d2}) \end{bmatrix} \\ u_{q1} = \frac{-1}{a_{3N}^2 - a_{4N}^2} \times \begin{bmatrix} a_{3N}f_{N3} + a_{4N}f_{N5} + \hat\theta^T(a_{3N}\alpha_3 + a_{4N}\alpha_5) \\ + k_q(a_{3N}s_{q1} + a_{4N}s_{q2}) + \lambda_q(a_{3N}e_{q1} + a_{4N}e_{q2}) \\ - a_{3N}\frac{di_{q1}^*}{dt} - a_{4N}\frac{di_{q2}^*}{dt} \end{bmatrix} \\ u_{q2} = \frac{-1}{a_{3N}^2 - a_{4N}^2} \times \begin{bmatrix} a_{4N}f_{N3} + a_{3N}f_{N5} + \hat\theta^T(a_{4N}\alpha_3 + a_{3N}\alpha_5) \\ + k_q(a_{4N}s_{q1} + a_{3N}s_{q2}) + \lambda_q(a_{4N}e_{q1} + a_{3N}e_{q2}) \\ - a_{4N}\frac{di_{q1}^*}{dt} - a_{3N}\frac{di_{q2}^*}{dt} \end{bmatrix} \end{cases} \quad (16)$$

Then, the update law for the uncertain parameters can be estimated as

$$\frac{d\hat\theta}{dt} = P^{-1}(e_\omega\alpha_1 + s_{d1}\alpha_2 + s_{d2}\alpha_4 + s_{q1}\alpha_3 + s_{q2}\alpha_5 - k_\theta\tilde\theta) \quad (17)$$

Substituting equations (16) and (17) into (15), the expression for H_2 can be simplified as

$$\begin{aligned} H_2 &= -(k_\omega - \frac{1}{\gamma^2} - \frac{1}{2})e_\omega^2 - k_d s_{d1}^2 - k_d s_{d2}^2 - k_q s_{q1}^2 - k_q s_{q2}^2 \\ &\quad - k_\theta \tilde{\theta}^T \tilde{\theta} - (\frac{\gamma}{2} d + \frac{e_\omega}{\gamma})^2 - \frac{\gamma^2}{4} d^2 + a_{1N} e_\omega (e_{q1} + e_{q1}) \\ &= -z_1^T Q z_1 - z_2^T Q z_2 - k_d s_{d1}^2 - k_d s_{d2}^2 - (\frac{\gamma}{2} d + \frac{e_\omega}{\gamma})^2 \\ &\quad - k_\theta \tilde{\theta}^T \tilde{\theta} - \frac{\gamma^2}{4} d^2 \le 0 \end{aligned} \tag{18}$$

where $z_1 = [e_\omega \; e_{q1} \int_0^t e_{q1} d\tau]^T$, $z_2 = [e_\omega \; e_{q2} \int_0^t e_{q2} d\tau]^T$; Q is a positive definite matrix with the following form.

$$Q = \begin{bmatrix} k_\omega/2 - 1/2\gamma^2 - 1/4 & 0 & 0 \\ -a_{1N} & k_q & 0 \\ 0 & 2k_q\lambda_q & k_q\lambda_q^2 \end{bmatrix}$$

Redefine the Lyapunov function $V = 2V_2$, and it follows readily

$$\frac{dV}{dt} = 2\frac{dV_2}{dt} \le \gamma^2 \|d\|^2 - \|e_\omega\|^2 \tag{19}$$

In turn, it can be shown that the consequent dissipative inequality (20) for a six-phase PMSM closed-loop system is obtained by integrating the both sides of inequality (19). Hence, the PMSM drive system has L_2 gain from the load disturbances to its tracking error.

$$V(t) - V(0) \le \int_0^t (\gamma^2 \|d\|^2 - \|e_\omega\|^2) d\tau \tag{20}$$

Remark 1: The physical meaning of dissipative inequality (20) is that all increased energy of six-phase PMSM drive system is always smaller than or equal to the ones from outside for any final time $t > 0$, i.e., the energy of six-phase PMSM system is decreasing.

In view of the dissipative inequality (20) holding, one can conclude that the closed-loop system is asymptotically stable as $d = 0$, furthermore, the L_2 gain from the load disturbances to the tracking error of drive system is smaller than or equal to γ as $d \neq 0$. Therefore, with the tracking and estimation errors close to zero as $t \to \infty$, L_2 gain for the load disturbances uniformly bounded with constant γ, it can realize the targets of speed tracking and disturbance rejection. Based on the above analysis, the block diagram of the robust ABSMC for the six-phase dual Y shift 30° surface-mounted PMSM system is shown in Fig. 1.

B. DESIGN OF RWFNN UNCERTAINTY OBSERVER

Considering that it is difficult to gain information on the lumped uncertainty θ during the practical applications of six-phase PMSM system, the on-line estimation compensation of the parametric perturbations has a significant effect on the control performance. Although the update law of the uncertain parameters shown in (17) can be implemented

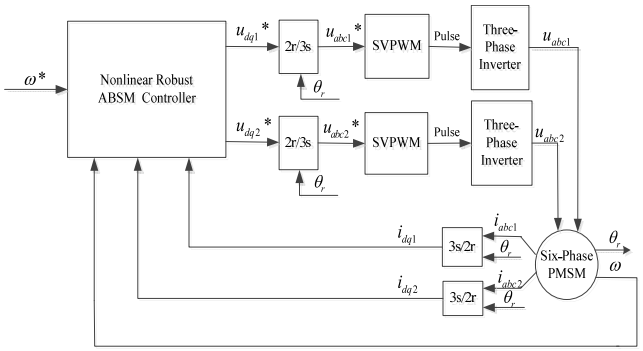

FIGURE 1. Block diagram of six-phase PMSM drive system using robust ABSM controller.

to achieve the convergence requirement of tracking error in the robust ABSMC law, this adaptation method has the problem of parameter tuning during the estimation of uncertainty information, which needs to be resolved by trial and error. In addition, this method cannot provide enough anti-interference robustness in practical applications. Therefore, a RWFNN uncertainty observer is proposed for the real-time estimation of the unknown in the following section to alleviate the aforementioned drawbacks.

The architecture of a five-layer RWFNN including the input layer (layer 1), membership layer (layer 2), rule layer (layer 3), wavelet and consequent layer (layer 4), and output layer (layer 5) is shown in Fig.2 [15]. The signal propagation and basic function in each layer of the RWFNN are introduced below.

1) Input layer: For every node in this layer, directly connected to various components of the inputs, the node input and output are represented as

$$\begin{cases} net_i^1 = x_i^1 \\ y_i^1 = f_i^1(net_i^1) = net_i^1; \quad i = 1, 2 \end{cases} \tag{21}$$

where $x^1 = [x_1^1 \quad x_2^1]^T = [e_\omega \quad \frac{de_\omega}{dt}]^T$, refers to network input variables.

2) Membership layer: In this layer, each node performs a membership function. Assuming Gaussian function as the membership function, one can gain the input and output of the jth node.

$$\begin{cases} net_{ij}^2 = -\dfrac{(y_i^1 - c_{ij})^2}{(b_{ij})^2} \\ y_{ij}^2 = f^2(net_{ij}^2) = \exp(net_{ij}^2); \quad j = 1, 2 \ldots m \end{cases} \tag{22}$$

where c_{ij} and b_{ij} are the mean and the standard deviation of the Gaussian in the jth membership function node with respect to the ith input variable, respectively; and m is the total number of nodes in the membership layer.

3) Rule layer: Each node in this layer is denoted by $\prod$, which multiplies the input signals and outputs the result of product. For the kth rule node in this layer, the input and

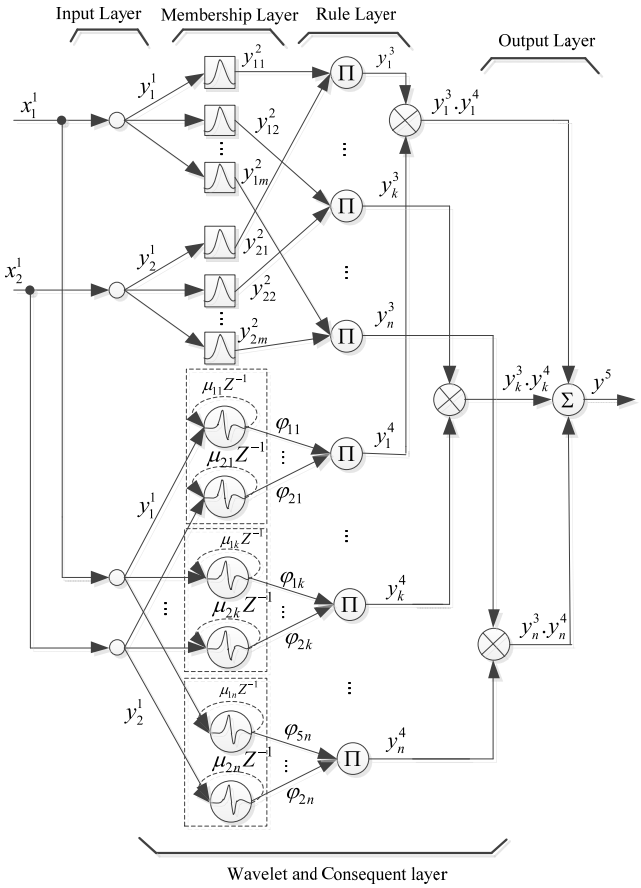

FIGURE 2. Network structure of RWFNN.

output are expressed as

$$\begin{cases} net_k^3 = \prod_{i=1}^{5} w_{jk}^3 y_{ij}^2 \\ y_k^3 = f^3(net_k^3) = net_k^3; \quad k = 1, 2 \ldots n \end{cases} \tag{23}$$

where the connecting weight w_{jk}^3, selected as the unit function, is the output action strength of the kth rule associated with the jth membership note; $n = m^5$ is the number of rules with complete rule connection if each input node has the same linguistic variables.

4) Wavelet and consequent layer: In the paper, the Gaussian wavelet function is adopted as a mother wavelet. Considering the recurrent structure, the input and output of the wavelet layer are

$$\begin{cases} net_k^4 = x_i^1 \\ u_{ik} = x_i^1 + \mu_{ik}\varphi_{ik} \\ \varphi_{ik} = (\dfrac{u_{ik} - t_{ik}}{d_{ik}}) \exp[\dfrac{-(u_{ik} - t_{ik})^2}{2d_{ik}^2}] \\ y_k^4 = \prod_{i=1}^{5} \varphi_{ik} \end{cases} \tag{24}$$

where t_{ik} and d_{ik} are the associated translation and dilation parameters of the wavelet function, respectively; and μ_{ik} is the recurrent feedback gain for dynamic information storage. Afterwards, the output of the consequent layer can be written as $y_k^3 y_k^4$.

5) Output layer: As the terminal layer of the RWFNN, the output layer is labelled with $\sum$, which will compute the overall output as the summation of all input signals. The final output of the network is

$$\begin{cases} net_l^4 = \sum_{k=1}^{n} W_{kl} y_k^3 y_k^4 \\ \hat{\theta}_l = f^4(net_l^4) = net_l^4; \quad l = 1, 2 \ldots 7 \end{cases} \tag{25}$$

where w_{kl}^4 refers to the weight between the network output layer and the consequent layer node.

The error function of the uncertainty observer utilizing the RWFNN is defined as

$$E = \tilde{\theta}^T \tilde{\theta}/2 \tag{26}$$

where $\tilde{\theta} = \hat{\theta} - \theta$ is the approximation error of the network.

The wavelet function and membership function parameters can be adjusted through the chain rule and gradient descent method, generally referred to as the BP learning algorithm. Therefore, the update laws of parameter adjustments in the membership and wavelet layer are designed as follows.

1) Output layer: In this layer, the error term to be propagated is calculated as

$$\delta_l^5 = -\frac{\partial E}{\partial \hat{\theta}} = -\frac{\partial E}{\partial \tilde{\theta}} \frac{\partial \tilde{\theta}}{\partial \hat{\theta}} = -\tilde{\theta}^T \tag{27}$$

2) Wavelet and consequent layer: The error term to be propagated is given by

$$\delta_k^4 = -\frac{\partial E}{\partial y_k^4} = -\frac{\partial E}{\partial \hat{\theta}} \frac{\partial \hat{\theta}}{\partial y_k^4} = \delta_l^5 [W_{k1} \ldots W_{k9}]^T y_k^3 \tag{28}$$

and the parameters of the wavelet function are updated by the amount

$$\begin{cases} \Delta t_{ik} = -\eta \dfrac{\partial E}{\partial t_{ik}} = -\eta \dfrac{\partial E}{\partial y_k^4} \dfrac{\partial y_k^4}{\partial \varphi_{ik}} \dfrac{\partial \varphi_{ik}}{\partial z_{ik}} \dfrac{\partial z_{ik}}{\partial t_{ik}} \\ \qquad = \dfrac{-\eta \delta_k^4 y_k^4}{d_{ik}} (\dfrac{1}{z_{ik}} - z_{ik}) \\ \Delta d_{ik} = -\eta \dfrac{\partial E}{\partial d_{ik}} = -\eta_d \dfrac{\partial E}{\partial y_k^4} \dfrac{\partial y_k^4}{\partial \varphi_{ik}} \dfrac{\partial \varphi_{ik}}{\partial z_{ik}} \dfrac{\partial z_{ik}}{\partial d_{ik}} \\ \qquad = \dfrac{-\eta \delta_k^4 y_k^4}{d_{ik}} (1 - z_{ik}^2) \\ \Delta \mu_{ik} = -\eta \dfrac{\partial E}{\partial \mu_{ik}} = -\eta \dfrac{\partial E}{\partial y_k^4} \dfrac{\partial y_k^4}{\partial \varphi_{ik}} \dfrac{\partial \varphi_{ik}}{\partial z_{ik}} \dfrac{\partial z_{ik}}{\partial \mu_{ik}} \\ \qquad = \dfrac{\eta \delta_k^4 y_k^4 \varphi_{ik}}{d_{ik}} (\dfrac{1}{z_{ik}} - z_{ik}) \end{cases} \tag{29}$$

The parameters in the wavelet layer are updated according to the following equation.

$$\begin{cases} t_{ik}(N) = t_{ik}(N-1) + \Delta t_{ik} + \alpha(t_{ik}(N-1) - t_{ik}(N-2)) \\ d_{ik}(N) = d_{ik}(N-1) + \Delta d_{ik} \\ \qquad + \alpha(d_{ik}(N-1) - d_{ik}(N-2)) \\ \mu_{ik}(N) = \mu_{ik}(N-1) + \Delta \mu_{ik} \\ \qquad + \alpha(\mu_{ik}(N-1) - \mu_{ik}(N-2)) \end{cases} \tag{30}$$

where the factors η and α are the learning rate and inertia term, respectively.

3) Rule layer: In consideration of the constant connecting weight w_{jk}^3, only the error term needs to be computed and propagated

$$\delta_k^3 = -\frac{\partial E}{\partial y_k^3} = -\frac{\partial E}{\partial \hat{\theta}}\frac{\partial \hat{\theta}}{\partial y_k^3} = \delta_l^5[W_1^T y_1^4 \dots W_n^T y_n^4]^T \tag{31}$$

4) Membership layer: The error term to be propagated is given by

$$\delta_{ij}^2 = -\frac{\partial E}{\partial y_{ij}^2} = -\frac{\partial E}{\partial y_k^3}\frac{\partial y_k^3}{\partial y_{ij}^2} = \delta_k^3 \frac{y_k^3}{y_{ij}^2} \tag{32}$$

By using of the chain rule, the parameters in this layer are updated by the amount

$$\begin{cases} \Delta c_{ij} = -\eta \dfrac{\partial E}{\partial c_{ij}} = -\eta \dfrac{\partial E}{\partial y_{ij}^2}\dfrac{\partial y_{ij}^2}{\partial net_{ij}^2}\dfrac{\partial net_j^2}{\partial c_{ij}} \\ \qquad = \eta \delta_{ij}^2 y_{ij}^2 \dfrac{2(y_i^1 - c_{ij})}{b_{ij}^2} \\ \Delta b_{ij} = -\eta \dfrac{\partial E}{\partial b_{ij}} = -\eta \dfrac{\partial E}{\partial y_{ij}^2}\dfrac{\partial y_{ij}^2}{\partial net_{ij}^2}\dfrac{\partial net_{ij}^2}{\partial b_{ij}} \\ \qquad = \eta \delta_{ij}^2 y_{ij}^2 \dfrac{2(y_i^1 - c_{ij})^2}{b_{ij}^3} \end{cases} \tag{33}$$

The update laws of parameters in the membership layer are

$$\begin{cases} c_{ij}(N) = c_{ij}(N-1) + \Delta c_{ij} + \alpha(c_{ij}(N-1) - c_{ij}(N-2)) \\ b_{ij}(N) = b_{ij}(N-1) + \Delta b_{ij} + \alpha(b_{ij}(N-1) - b_{ij}(N-2)) \end{cases} \tag{34}$$

A large learning rate η can reduce the required learning time of the network, but it may cause oscillation in the learning process due to the excessive adjustment of gradient descent method. Based on the approximation error index function, an adaptive learning rate adjustment algorithm is presented as follows.

$$\begin{cases} \eta(N+1) = 1.1\eta(N) & if\ E(N+1) < E(N) \\ \eta(N+1) = 0.8\eta(N) & if\ E(N+1) > 1.05E(N) \\ \eta(N+1) = \eta(N) & else \end{cases} \tag{35}$$

To develop the adaptation update law for the RWFNN uncertainty observer, the network output $\hat{\theta}$ and minimum approximation error $\tilde{\theta}_{\min}$ can be defined as

$$\begin{aligned} \hat{\theta} &= W^T \Gamma \\ \tilde{\theta}_{\min} &= W_*^T \Gamma - \theta \end{aligned} \tag{36}$$

where $\Gamma = [y_1^3 y_1^4 \dots y_n^3 y_n^4]^T$, W_* is the optimal weight vector that achieves the minimum approximation error.

The following Lyapunov function V_3 is chosen to prove the stability of the proposed control system.

$$V_3 = V_1 + \frac{1}{2}s_{d1}^2 + \frac{1}{2}s_{d2}^2 + \frac{1}{2}s_{q1}^2 + \frac{1}{2}s_{q2}^2 + \frac{1}{2\rho_1}\left\|\tilde{W}\right\|^2 \tag{37}$$

In view of $\|\tilde{W}\|^2 = tr(\tilde{W}^T\tilde{W})$, augmenting the energy function $H_3 = \frac{dV_3}{dt} + \frac{1}{2}(\|e_\omega\|^2 - \gamma^2\|d\|^2)$ and using the designed control law shown in (16), one can obtain

$$\begin{aligned} H_3 &= -z_1^T Q z_1 - z_2^T Q z_2 - k_d s_{d1}^2 - k_d s_{d2}^2 - (\frac{\gamma}{2}d + \frac{e_\omega}{\gamma})^2 \\ &\quad - \frac{\gamma^2}{4}d^2 + \frac{1}{2\rho_1}\frac{d\left\|\tilde{W}\right\|^2}{dt} \\ &\quad - \tilde{\theta}^T(e_\omega\alpha_1 + s_{d1}\alpha_2 + s_{d2}\alpha_4 + s_{q1}\alpha_3 + s_{q2}\alpha_5) \\ &= -z_1^T Q z_1 - z_2^T Q z_2 - k_d s_{d1}^2 - k_d s_{d2}^2 - (\frac{\gamma}{2}d + \frac{e_\omega}{\gamma})^2 \\ &\quad - \frac{\gamma^2}{4}d^2 + \frac{1}{\rho_1}tr((\frac{d\tilde{W}}{dt})^T\tilde{W} - \rho_1 K\Gamma^T\tilde{W}) - \tilde{\theta}_{\min}^T K \end{aligned} \tag{38}$$

where $K = e_\omega\alpha_1 + s_{d1}\alpha_2 + s_{d2}\alpha_4 + s_{q1}\alpha_3 + s_{q2}\alpha_5$; $\tilde{W} = W - W_*$ is defined as the estimation error of the network weight; ρ_1 is a positive constant.

The following adaptation update law for the network weight estimation is

$$\frac{dW}{dt} = \rho_1 \Gamma K^T \tag{39}$$

Thus, the energy function H_3 is uniformly bounded with the bounded norms of $\tilde{\theta}_{\min}$ and K as $t \to \infty$. In addition, the RWFNN structure should be optimized such that $\tilde{\theta}_{\min}$ is sufficiently small to guarantee $H_3 \le 0$ for the practical stability operation of six-phase PMSM closed-loop system. Fig. 3 shows the block diagram of the robust ABSM controller based on the RWFNN uncertainty observer.

Remark 2: It is noted that the compensation mechanism of unknown parameters is derived from the universal approximation property of the RWFNN shown in (25) and (39), other than the adaptation method shown in (17). That is to say, the RWFNN observer actually substitutes for the adaptation technique in the ABSMC with RWFNN to improve the robustness and parameter insensitivity. Additionally, the proposed nonlinear controller with the robust ABSMC law and RWFNN uncertainty observer can ensure that the speed tracking error tends to zero, but it does not imply a convergence of the lumped uncertainty estimation to its real value.

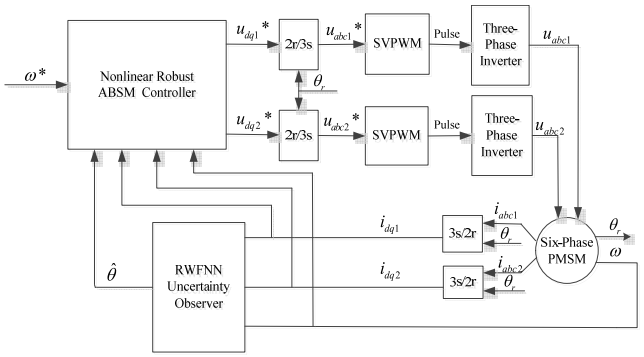

FIGURE 3. Block diagram of robust ABSM controller with RWFNN uncertainty observer.

TABLE 1. Specifications of six-phase PMSM.

Parameter	Value
Rated Power (PN)	3.1 [kW]
Rated Speed (nN)	1000 [r·min^{-1}]
Rated Torque (TN)	30 [N.m]
Number of Pole Pairs (npN)	4
Damping Coefficient (BwN)	0.001 [N.m/(rad/s)]
Stator Resistance (RsN)	2.875 [Ω]
Stator Inductance (LN)	8.5 [mH]
Mutual Inductance (LmN)	8 [mH]
Flux Linkage(φ_{fN})	0.175[Wb]
Motor Inertia (JN)	0.08 [kg·m^2]

IV. SIMULATION RESULTS

To demonstrate the validity of the proposed control strategy, simulations on the six-phase dual Y shift 30° surface-mounted PMSM speed drive system have been performed using Matlab/Simulink software. The voltage source inverter is represented by its equivalent model so that switching effects are not considered. Table 1 shows the nominal parameters of the six-phase PMSM used in the simulations.

In consideration of the influence on the speed regulation and current responses under the parameter perturbations and load disturbances, the uncertainty parameters introduced in the six-phase PMSM drive system are set as follows: $R_s = 1.2R_{sN}$, $L = 1.2L_N$, $L_m = 1.2L_{mN}$, $J = 1.5J_N$, $\psi_f = 0.8\psi_{fN}$, and $B_\omega = 2B_{\omega N}$. The simulation results of the robust ABSM controller with the speed reference command $n^* = 1000\text{r} \cdot \text{min}^{-1}$ and different load torque terms for piecewise constants and fast variations are given hereinafter, respectively. More specifically, to present the effect of the electromagnetic parameter variations (R_s, L, and L_m) on the dynamic responses of the stator currents (with i_{d1}, i_{q1} as the cases), Figs. 4 and 5 depict the simulation comparison results of the stator current tracking under the nominal parameters and uncertainty parameters. Likewise, the effect of the mechanical parameter variations (J, B_ω) on the dynamic speed response for the PMSM drive system is also presented in Figs. 4 and 5.

From the simulation results shown in Figs. 4 and 5, it can be observed that despite the influence on the speed regulation and current responses under the parameter uncertainty and external load disturbances is severe, the system speed, stator currents, and electromagnetic torque still possess the good steady and dynamic features, such as the steady state error

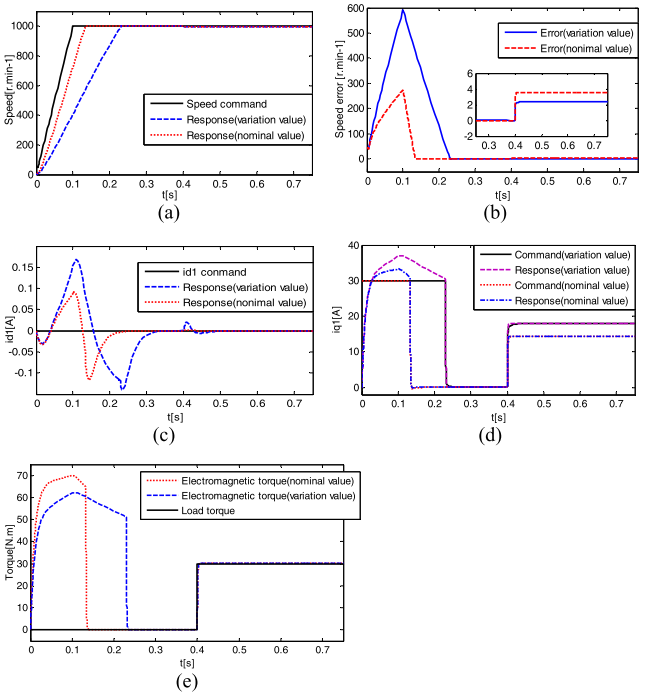

FIGURE 4. Simulation under robust ABSM controller with piecewise constant load. (a) Speed reference and response. (b) Speed error. (c) i_{d1} reference and response. (d) i_{q1} reference and response. (e) Load and electromagnetic torque.

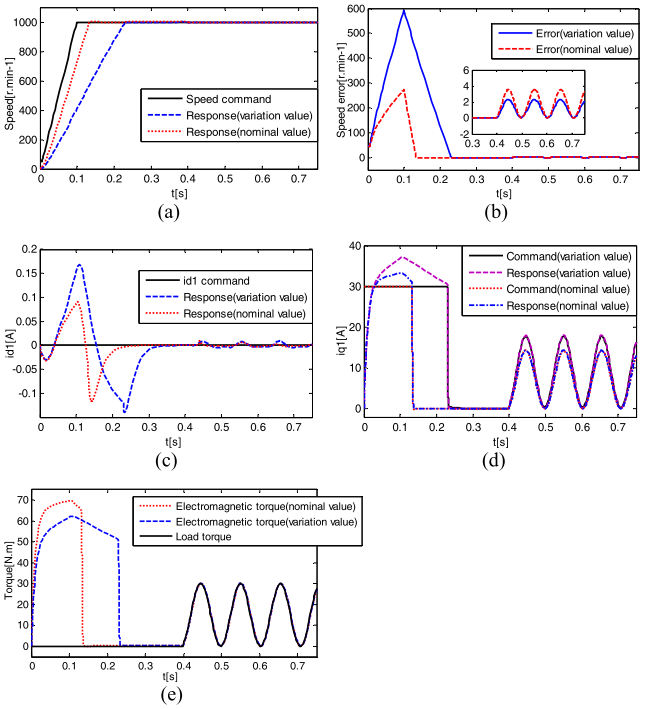

FIGURE 5. Simulation under robust ABSM controller with fast-varying load. (a) Speed reference and response. (b) Speed error. (c) i_{d1} reference and response. (d) i_{q1} reference and response. (e) Load and electromagnetic torque.

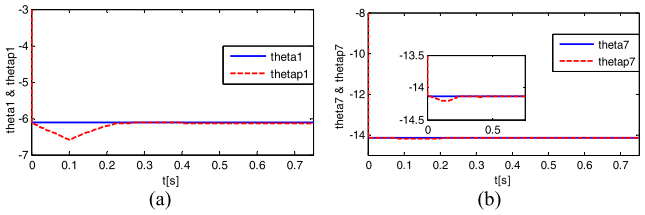

FIGURE 6. Simulation of uncertainty parameters estimation. (a) Parameter θ_1 with its estimated value. (b) Parameter θ_7 with its estimated value.

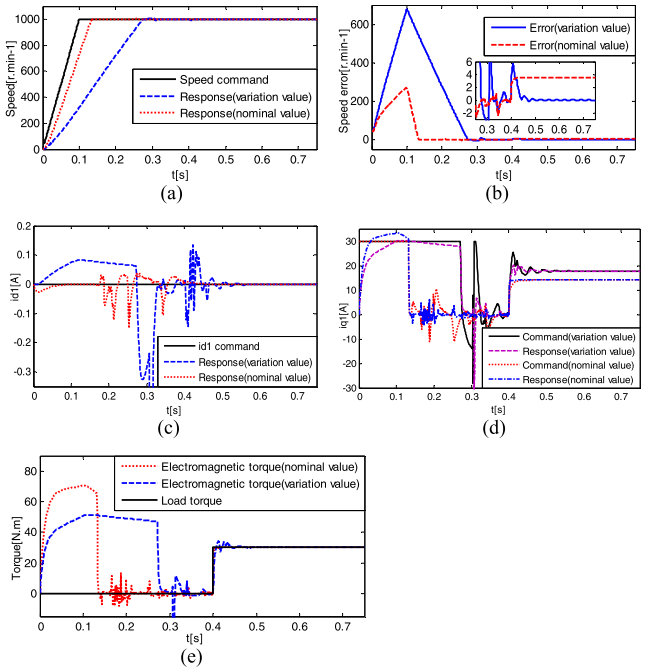

FIGURE 7. Simulation under robust ABSM controller using RWFNN uncertainty observer with piecewise constant load. (a) Speed reference and response. (b) Speed error. (c) i_{d1} reference and response. (d) i_{q1} reference and response. (e) Load and electromagnetic torque.

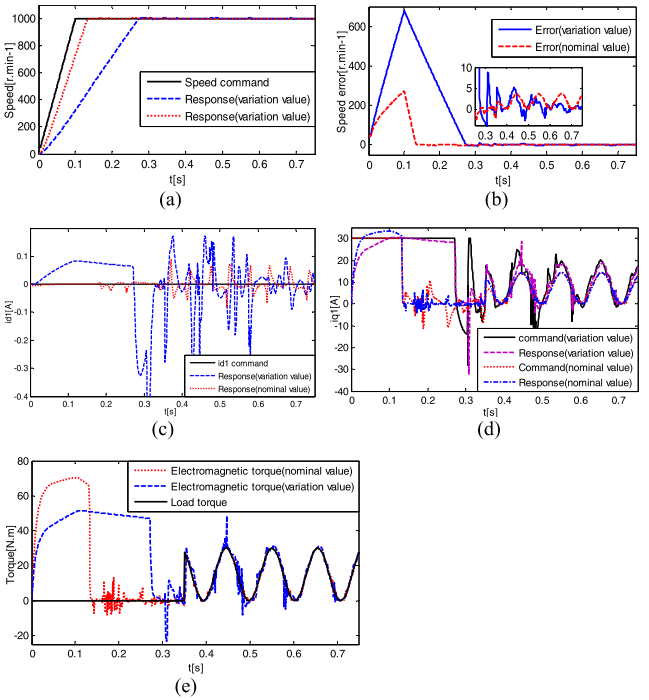

FIGURE 8. Simulation under robust ABSM controller using RWFNN uncertainty observer with fast-varying load. (a) Speed reference and response. (b) Speed error. (c) i_{d1} reference and response. (d) i_{q1} reference and response. (e) Load and electromagnetic torque.

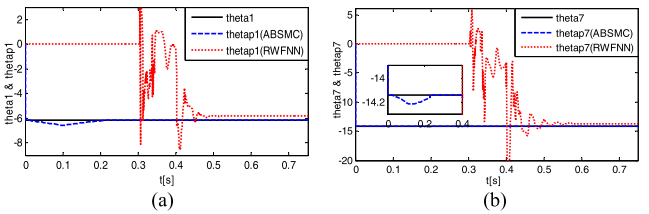

FIGURE 9. Simulation comparison of uncertainty parameters estimation with two control schemes. (a) Parameter θ_1 with its estimated value. (b) Parameter θ_7 with its estimated value.

close to zero, short settling time, high control accuracy, and obscure oscillation etc., which indicates that the proposed nonlinear speed controller using the robust ABSMC method has the ability to realize speed tracking and uncertain disturbance suppression. It is worth mentioning that the effect of load disturbances on tracking output is attenuated apparently, whether it is with wide range of changes or fast variations. In addition, the results, shown in Fig. 6, reveal that the uncertainty adaptation law can completely compensate the parameter perturbations. Its estimated value for uncertain parameters (with $\hat{\theta}_1$, $\hat{\theta}_7$ as the cases) can gradually converge to the real value.

In order to verify the effective approximation characteristics of the RWFNN, the simulation results of the ABSMC with the RWFNN uncertainty observer (the simulation and uncertainty conditions are the same as above) are depicted in Figs. 7 and 8. Note that the effect of the parameter variations on the dynamic speed and current responses is also given hereinafter. Likewise, the main difference between two proposed methods lies in the on-line adaption mechanism of unknown parameters, and the estimation processes (with $\hat{\theta}_1, \hat{\theta}_7$ as the cases) of both control schemes are provided simultaneously for a comprehensive comparison in Fig. 9.

Simulation results indicate that the robust ABSM control law with the RWFNN uncertainty observer can guarantee high speed tracking precision and uncertain disturbance rejection, i.e., speed response has a smaller tracking error in the uncertainty conditions compared with the speed controller proposed above. Besides, when there are load disturbances with wide range of changes or fast variations, the dynamic responses of system torque have the smaller overshoot, which can relieve electromagnetic impact and mechanical damage caused by excessively large and long overshoot. It can be found that the compensation mechanism adopted by the RWFNN cannot guarantee a convergence of the lumped uncertainty estimation to its real value, but a bounded estimation error. However, the interference robustness of the PMSM system is not affected much. Therefore, with the

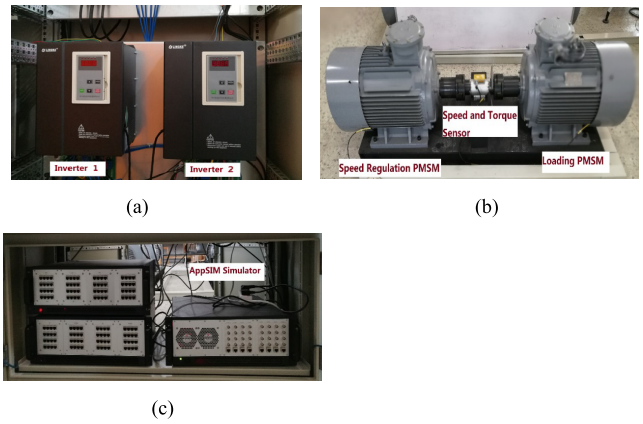

(a) (b) (c)

FIGURE 10. PMSM prototype system experimental platform. (a) Two inverters. (b) Two PMSMs and speed-torque sensor. (c) AppSIM simulator.

RWFNN uncertainty observer, the robust ABSM controller can effectively improve the anti-interference robustness and parameter insensitivity of the six-phase PMSM drive system.

V. EXPERIMENTAL RESULTS

A. EXPERIMENTAL SYSTEM SETUP

To practically evaluate the actual performance of the proposed control scheme, a prototype PMSM speed control experimental platform is built and tested using AppSIM real-time simulator (the specific parameters of six-phase PMSM prototype system are the same as above, listed in the Table 1). As shown in Fig. 10, the realized system is composed of a personal computer (PC), an AppSIM simulator, a PCI signal acquisition board with an A/D-D/A card, two inverters and PMSMs of the same type. The speed regulation PMSM corresponding with the first inverter tracks the speed reference trajectory given by the upper computer. The loading PMSM connected to the speed regulation PMSM is controlled by the second inverter to realize the load torque simulation of the motor drive system. As the system controller, the AppSIM simulator mainly performs the operation of algorithm implementation, generation of SVPWM wave and communication with the PC.

In the proposed control system, all the programs are developed using the 'Matlab' language in the AppSIM simulator environment and then compiled into the 'C' and 'Assembly' languages for the implementation of the IGBT modules-based inverter. In the real-time control procedure, input/output and network initialization parameters are set first. Then, the programs with 1ms sample interval of the speed control loop are used for the speed-torque sensor (the minimum speed measurement of the JN338 sensor used in the experimental setup is $0.5\%*F \cdot S = 1500*0.5\% = 7.5\,r \cdot min^{-1}$) and the signal acquisition board. Next, the tracking errors and current commands are generated according to the presented control algorithm. The sampling interval of the current control loops is set as 0.1ms for reading the stator currents and computing the voltage commands. Ultimately, the calculated commands of SVPWM technology are sent to the inverter of six-phase PMSM speed drive system. The

TABLE 2. Experimental results of motor system under piecewise constant load disturbance.

Indexes \ Controllers		PI	ABSM	RABSM	RABSM+ RWFNN
Ts (s)	0.00-0.35s	0.33	0.26	0.24	0.22
	0.35-0.55s	0.15	0.08	0.05	0.03
	0.55-0.75s	0.17	0.13	0.08	0.07
O (%)	0.00-0.35s	1.08	2.52	1.04	0.57
	0.35-0.55s	3.26	1.97	1.50	0.91
	0.55-0.75s	3.56	2.83	3.05	3.08
Es (r/min)	0.00-0.35s	1.03	0.17	0.13	0.13
	0.35-0.55s	20.2	9.64	7.01	4.12
	0.55-0.75s	21.1	16.1	10.3	6.15

parameters and specifications of the LK600 inverter adopted in the PMSM drive system are summarized as follows: rated power $P_{inv} = 3.7$kW, rated alternating voltage $U_{inv} =$ 200-230V, rated current $I_{inv} = 17$A. Moreover, the DC-bus voltage is 400V and the sampling frequency of SVPWM (also called the switching frequency of inverter) is set as 10 kHz.

B. EXPERIMENTAL RESULTS

In order to validate the speed control performance of the proposed ABSMC and the anti-interference robustness of the RWFNN observer in the condition of the dynamic load perturbations, the following test cases are designed with the different load torque terms for piecewise constants and fast variations. The startup procedure of the drive system is implemented when the reference speed is given as $1000r \cdot min^{-1}$ with no-load test first. With the system running at a steady state, different load torque terms for piecewise constants and fast variations are added to the system suddenly at $t = 0.35$s. Hereafter, the reference speed command is decreased from $1000r \cdot min^{-1}$ to $800r \cdot min^{-1}$ at $t = 0.55$s. For a comprehensive analysis of the control performance, the experimental results of the motor speed, q axis current, and torque responses obtained using the PI controller, traditional ABSMC, and two proposed controllers (RABSMC and RABSMC+RWFNN) are presented in Figs. 11-12. In addition, there are some performance indexes introduced in this work, such as settling time (Ts), overshoot (O), steady state error (Es), and ripple coefficient (Rc). And a comparison of performance indexes on the four methods are provided in Tables 2–3. Additionally, to measure the control performance of the proposed control scheme on the whole, the maximum tracking error T_{ma}, the average tracking error T_{av}, and the standard deviation of tracking error T_{sd} for the speed trajectory tracking are introduced as follows [11].

$$T_{ma} = \max_{1 \le n \le N} |e_\omega(nT)|$$

$$T_{av} = \frac{\sum_{n=1}^{N} |e_\omega(nT)|}{N}$$

$$T_{sd} = \sqrt{\frac{\sum_{n=1}^{N} [|e_\omega(nT)| - T_a]^2}{N}}$$

TABLE 3. Experimental results of motor system under fast-varying load disturbance.

Indexes \ Controllers		PI	ABSM	RABSM	RABSM+ RWFNN
Ts (s)	0.00-0.35s	0.32	0.29	0.25	0.23
	0.35-0.55s	-	0.08	0.06	0.06
	0.55-0.75s	-	0.15	0.11	0.08
O (%)	0.00-0.35s	1.09	2.52	1.04	0.82
	0.35-0.55s	2.71	1.90	1.44	0.66
	0.55-0.75s	3.81	2.39	1.21	1.10
Rc (%)	0.00-0.35s	1.09	1.82	1.82	1.07
	0.35-0.55s	2.98	1.08	0.96	1.24
	0.55-0.75s	3.85	1.47	0.76	1.16

Additionally, all the parameters of the PI controller, ABSM controller, and two proposed controllers are selected by the trial and error method to achieve the best transient control performance considering the requirement of stability and robustness. Moreover, all the parameter values trained online in the RWFNN are initialized with zero. Consequently, the specific parameters in the experiment are given as follow.

$$k_{n\_P} = 5;\ k_{n\_I} = 0.3;\ k_{id\_P} = k_{iq\_P} = 8;\ k_{id\_I} = k_{iq\_I} = 15;$$
$$k_{\omega} = 500;\ \gamma = 0.1;\ \lambda_d = \lambda_q = 50;\ k_d = k_q = 100;$$
$$k_{\theta} = 1000;\ P = 0.1^{*} I_{7\times 7}.$$

As shown in the experimental results, when the given speed and load torque are changed suddenly with different torque terms for piecewise constants and fast variations, the ABSMC strategies enable the system to have good characteristics such as the shorter settling time, smaller overshoot and steady state error, and obscure ripple coefficient. This is caused by the PI controller's sensitive dependence on the structure parameters and external disturbances. Besides, the distinct oscillation is aroused in the speed response of the traditional ABSMC under the external disturbances with fast variations by neglecting the dynamic process of dynamic load torque, thus deteriorating the quality of speed regulation system. Nevertheless, since the nonlinear H_∞ is utilized to minimize the influence of dynamic load disturbances on speed tracking output in this paper, the two proposed robust ABSM controllers can compensate the uncertainty impacts through designing adaptive control law and RWFNN uncertainty observer.

Compared with the robust ABSM controller, it can be seen that, the robust ABSMC law with RWFNN uncertainty observer exploits the RWFNN to approach the system uncertainty. Thus, on the premise of guaranteeing speed tracking precision, the motor speed response is featured by the smaller overshoot and steady state error. In addition, the smaller torque response can relieve electromagnetic impact and mechanical damage caused by excessively large and long torque overshoot. However, it should be noted that the memory burden and implementation complexity of the RWFNN observer are higher than the adaptation method. Hence, some extra efforts, including the use of chips with fast data processing capability and the optimization of network configuration parameters, are required to implement the proposed robust ABSMC with RWFNN uncertainty observer.

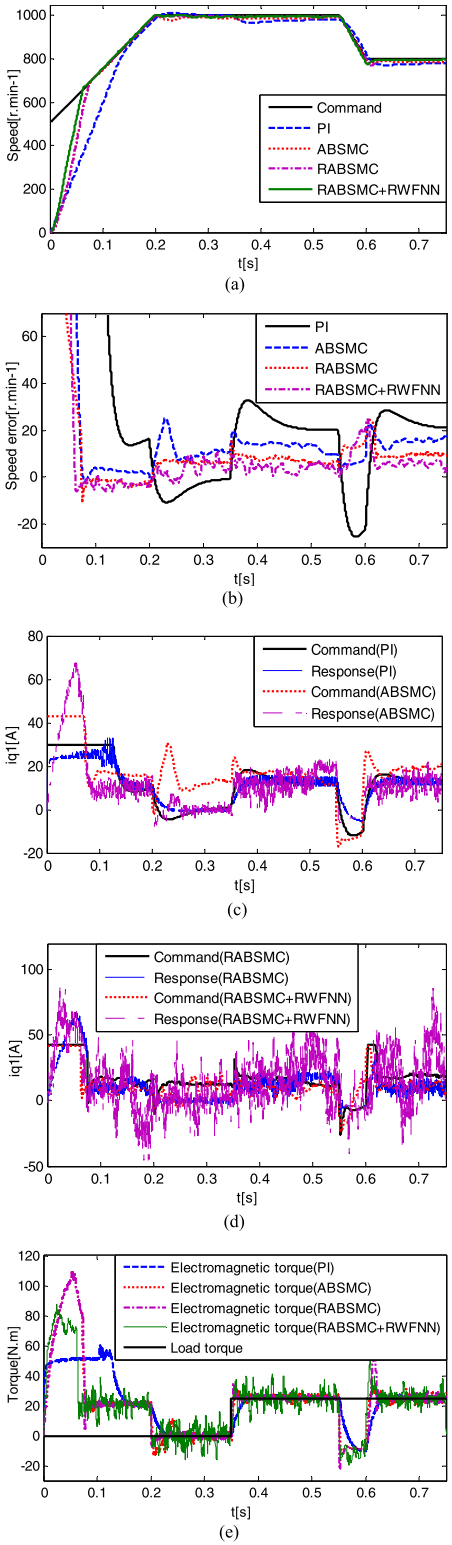

FIGURE 11. Experimental comparison of four controllers with piecewise constant load. (a) Speed reference and response. (b) Speed error. (c) i_{q1} reference and response. (d) i_{q1} reference and response. (e) Load and electromagnetic torque.

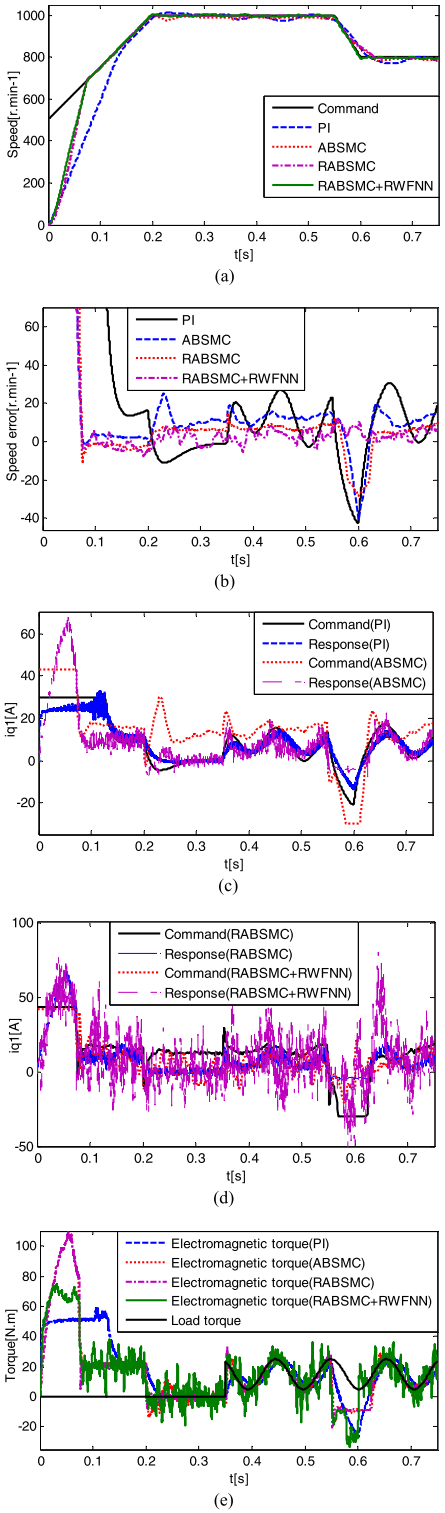

FIGURE 12. Experimental comparison of four controllers with fast-varying load. (a) Speed reference and response. (b) Speed error. (c) i_{q1} reference and response. (d) i_{q1} reference and response. (e) Load and electromagnetic torque.

Furthermore, the control performance of the various controllers under the piecewise constant and fast-varying load disturbances is shown in Fig. 13. The poor tracking responses

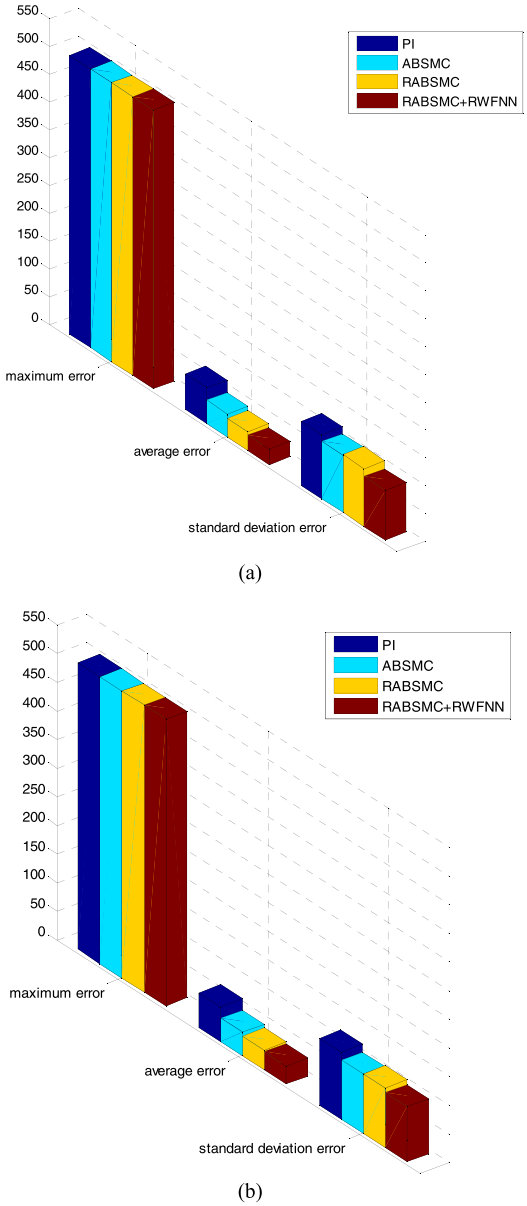

FIGURE 13. Performance indexes of four controllers. (a) Case 1 with piecewise constant load. (b) Case 2 with fast-varying load.

are resulted for the PI controller due to its fixed structure parameters. However, the ABSMC strategies can guarantee the high performance of speed trajectory tracking and lumped uncertainty suppression. Additionally, considering the effect of dynamic load disturbances on the speed response, the robust ABSM controller has been proposed to maintain the superior maximum, average, and standard deviation of tracking errors. On the other hand, the RWFNN uncertainty observer has been proposed to improve the anti-interference robustness and control performance owing to its advanced network structure and online learning scheme. Therefore, the proposed robust ABSM controller with RWFNN observer has the lower maximum, average, and standard deviation of the tracking errors at both test cases.

VI. CONCLUSION

This study proposes a robust ABSMC law with RWFNN observer for the speed regulation of a six-phase PMSM drive system demonstrating lumped uncertainty. First, the system mathematical model in the synchronous rotating reference frame is introduced. Then, the robust ABSM controller, that takes the integration of the speed loop and current loops with load disturbance rejection into account, is presented to compensate the uncertainty while maintaining speed tracking. Furthermore, to improve the anti-interference robustness and parameter insensitivity, the RWFNN observer is proposed for the real-time uncertainty compensation, and the online learning process of network parameters is designed. In addition, the proposed control scheme is implemented in an AppSIM real-time simulator and the validity of the proposed control algorithm is verified by simulations and experimental results.

REFERENCES

[1] S. H. Chang, P. Y. Chen, Y. H. Ting, and S. W. Hung, "Robust current control-based sliding mode control with simple uncertainties estimation in permanent magnet synchronous motor drive systems," *IET Electr. Power Appl.*, vol. 4, no. 6, pp. 441–450, Jul. 2010.

[2] H. Kim, J. Son, and J. Lee, "A high-speed sliding-mode observer for the sensorless speed control of a PMSM," *IEEE Trans. Ind. Electron.*, vol. 58, no. 9, pp. 4069–4077, Sep. 2011.

[3] F. J. Lin, I. F. Sun, K. J. Yang, and J. K. Chang, "Recurrent fuzzy neural cerebellar model articulation network fault-tolerant control of six-phase permanent magnet synchronous motor position servo drive," *IEEE Trans. Fuzzy Syst.*, vol. 24, no. 1, pp. 153–167, Feb. 2016.

[4] X. J. Ma, Y. X. Yu, H. Q. Zhang, W. Wang, and L. S. Liu, "Study on direct torque control of dual Y shift 30 degree six-phase PMSM," in *Proc. IEEE Conf. Ind. Electron Appl. (ICIEA)*, Jun. 2015, pp. 1964–1968.

[5] X. Zhang, L. Sun, K. Zhao, and L. Sun, "Nonlinear speed control for PMSM system using sliding-mode control and disturbance compensation techniques," *IEEE Trans. Power Electron.*, vol. 28, no. 3, pp. 1358–1365, Mar. 2013.

[6] A. R. Ghafari-Kashani, J. Faiz, and M. J. Yazdanpanah, "Integration of non-linear H_∞ and sliding mode control techniques for motion control of a permanent magnet synchronous motor," *IET Electr. Power Appl.*, vol. 4, no. 4, pp. 267–280, Apr. 2009.

[7] T. S. Lee, C. H. Lin, and F. J. Lin, "An adaptive H_∞ controller design for permanent magnet synchronous motor drives," *Control Eng. Pract.*, vol. 13, no. 4, pp. 425–439, 2005.

[8] Z. Chen, B. Yao, and Q. Wang, "Accurate motion control of linear motors with adaptive robust compensation of nonlinear electromagnetic field effect," *IEEE/ASME Trans. Mechatronics*, vol. 18, no. 3, pp. 1122–1129, Jun. 2013.

[9] M. Zbynek, V. Libor, and V. Pavel, "PMSM model predictive control with field-weakening implementation," *IEEE Trans. Ind. Electron.*, vol. 63, no. 8, pp. 5156–5166, Aug. 2016.

[10] H. X. Liu and S. H. Li, "Speed control for PMSM servo system using predictive functional control and extended state observer," *IEEE Trans. Ind. Electron.*, vol. 59, no. 2, pp. 1171–1183, Feb. 2012.

[11] F. J. Lin, Y. C. Hung, and M. T. Tsai, "Fault-tolerant control for six-phase PMSM drive system via intelligent complementary sliding-mode control using TSKFNN-AMF," *IEEE Trans. Ind. Electron.*, vol. 60, no. 12, pp. 5747–5762, Dec. 2013.

[12] Q. X. Jia, X. D. Zhang, and H. X. Sun, "Integral backstepping sliding-mode control for space manipulator modular joint using RBFN observer," in *Proc. IEEE Conf. Inform. Acquisit. (ICIA)*, Jul. 2007, pp. 385–390.

[13] C.-M. Lin and H.-Y. Li, "Intelligent control using the wavelet fuzzy CMAC backstepping control system for two-axis linear piezoelectric ceramic motor drive systems," *IEEE Trans. Fuzzy Syst.*, vol. 22, no. 4, pp. 791–802, Aug. 2014.

[14] L. F. Jesús, G. R. Carlos, S. R. Hebertt, and D. R. C. Oscar, "Robust backstepping tracking controller for low-speed PMSM positioning system: Design, analysis, and implementation," *IEEE Trans. Ind. Informat.*, vol. 11, no. 5, pp. 1130–1141, May 2015.

[15] F. J. Lin, Y. C. Hung, and K. C. Ruan, "An intelligent second-order sliding-mode control for an electric power steering system using a wavelet fuzzy neural network," *IEEE Trans. Fuzzy Syst.*, vol. 22, no. 6, pp. 1598–1611, Jun. 2014.

[16] F.-J. Lin, K.-J. Yang, I.-F. Sun, and J.-K. Chang, "Intelligent position control of permanent magnet synchronous motor using recurrent fuzzy neural cerebellar model articulation network," *IET Electric Power Appl.*, vol. 9, no. 3, pp. 248–264, 2015.

[17] S. Liu, Y. T. Zhang, and C. G. Yu, "Three-dimensional fuzzy control for ship electric propulsion turbine," *Proc. CSEE*, vol. 32, no. 3, pp. 117–123, 2012.

[18] K. Murat and I. E. Halil, "Design, modelling and simulation of a new nonlinear and full adaptive backstepping speed tracking controller for uncertain PMSM," *Appl. Math. Model.*, vol. 36, no. 11, pp. 5199–5213, 2012.

[19] J. Soltani and M. Pahlavaninezhad, "Adaptive backstepping based controller design for interior type PMSM using maximum torque per ampere strategy," in *Proc. IEEE Conf. Power Electron. Drive Syst. (PEDS)*, Dec. 2005, pp. 596–601.

[20] D. Jorge, "Exact tracking using backstepping control design and high-order siding modes," *IEEE Trans. Autom. Control*, vol. 58, no. 8, pp. 2077–2081, Aug. 2013.

[21] K. V. Prashanth and H. G. Navada, "Parameter estimation of PMSM using adaptive backstepping technique," in *Proc. IEEE Conf. Adv. Energy Technol. (ICAECT)*, Jan. 2014, pp. 1–6.

[22] Q. L. Viet, H. C. Han, and J. W. Jung, "Fuzzy sliding mode speed controller for PM synchronous motors with a load torque observer," *IEEE Trans. Power Electron.*, vol. 27, no. 3, pp. 1530–1539, Mar. 2012.

[23] C. F. Zhang, M. G. Niu, J. He, and K. H. Zhao, "Robust synchronous control of multi-motor integrated with artificial potential field and sliding mode variable structure," *IEEE Access*, vol. 5, pp. 197–207, 2017.

[24] F. J. Lin, C. K. Chang, and P. K. Huang, "FPGA-based adaptive backstepping sliding-mode control for linear induction motor drive," *IEEE Trans. Power Electron.*, vol. 22, no. 4, pp. 1222–1231, Jul. 2007.

[25] H. Lin, W. S. Yan, Y. T. Wang, B. Gao, and Y. Yao, "Nonlinear sliding mode speed control of a PM synchronous motor drive using model reference adaptive backstepping approach," in *Proc. IEEE Conf. Mechatron. Autom. (ICMA)*, Aug. 2009, pp. 828–833.

[26] P. H. Shen and F. J. Lin, "Intelligent backstepping sliding-mode control using RBFN for two-axis motion control system," *IEE Proc. Electr. Power Appl.*, vol. 152, no. 5, pp. 1321–1342, 2005.

[27] F. F. M. El-Sousy, "Robust wavelet-neural network sliding-mode control system for permanent magnet synchronous motor drive," *IET Electr. Power Appl.*, vol. 5, no. 1, pp. 113–132, 2011.

[28] X. Wen, X. Li, and E. S. Wang, "Observer design for the single hidden layer fuzzy recurrent wavelet neural network," *Chin. J. Radio Sci.*, vol. 30, no. 6, pp. 1197–1204, 2015.

[29] C. H. Lin, R. C. Wu, and C. C. Chong, "Adaptive backstepping control for a PMSM drive using RFNN uncertainty observer," in *Proc. IEEE Conf. Ind. Electron. Appl. (ICIEA)*, Jun. 2011, pp. 62–67.

[30] A. Wang, X. Jia, and S. Dong, "A new exponential reaching law of sliding mode control to improve performance of permanent magnet synchronous motor," *IEEE Trans. Magn.*, vol. 49, no. 5, pp. 2409–2412, May 2013.

[31] Y. Wang, X. Wen, and F. Zhao, "Vector control of six-phase PMSMs with selective harmonic elimination PWM," in *Proc. IEEE Trans. Electrific. Conf. Expo Asia–Pacific (ITEC Asia–Pacific)*, Sep. 2014, pp. 1–5.

[32] J. Yu, P. Shi, W. Dong, B. Chen, and C. Lin, "Neural network-based adaptive dynamic surface control for permanent magnet synchronous motors," *IEEE Trans. Neural Netw. Learn. Syst.*, vol. 26, no. 3, pp. 640–645, Mar. 2014.

[33] M. Yang, X. C. Wang, and K. Zheng, "Nonlinear controller design for permanent magnet synchronous motor using adaptive weighted PSO," in *Proc. Amer. Control Conf.*, 2010, pp. 1962–1966.

[34] A. V. Sant, K. R. Rajagopal, and N. K. Sheth, "Permanent magnet synchronous motor drive using hybrid PI speed controller with inherent and noninherent switching functions," *IEEE Trans. Mag.*, vol. 47, no. 10, pp. 4088–4091, Oct. 2013.

[35] M. Z. Qiao, C. Jiang, Y. X. Zhu, and G. Li, "Research on design method and electromagnetic vibration of six-phase fractional-slot concentrated-winding PM motor suitable for ship propulsion," *IEEE Access*, vol. 4, pp. 8535–8543, 2016.

[36] S. Liu and Y. Z. Cheng, "Modeling of a twelve-phase synchronous machine using Matlab/Simpowersystems," in *Proc. 2nd ICECC*, 2011, pp. 2131–2134.

[37] C. Zheng, Y. Bin, and Q. F. Wang, "μ-synthesis-based adaptive robust control of linear motor driven stages with high-frequency dynamics: A case study," *IEEE Trans. Mechatronics*, vol. 20, no. 3, pp. 1482–1490, Mar. 2015.
[38] F. J. Lin, Y. C. Hung, J. C. Hwang, and M. T. Tsai, "Fault-tolerant control of a six-phase motor drive system using a Takagi-Sugeno-Kang type fuzzy neural network with asymmetric membership function," *IEEE Trans. Power Electron.*, vol. 28, no. 7, pp. 3557–3572, Jul. 2013.
[39] S. Li, M. Zhou, and X. Yu, "Design and implementation of terminal sliding mode control method for PMSM speed regulation system," *IEEE Trans. Ind. Informat.*, vol. 9, no. 4, pp. 1879–1891, Nov. 2013.

LIU SHENG was born in Baicheng, China, in 1957. He received the B.Eng. degree in industrial automation from the Harbin University of Civil Engineering and Architecture, Harbin, China, in 1982, and the master's and Ph.D. degrees in theory and control engineering from Harbin Engineering University, Harbin, in 1982 and 2000, respectively. He is currently a Professor with Harbin Engineering University.

His current research interests include electromagnetic compatibility prediction and measurement, optimization estimate and control of random system, and robust control and ship control system.

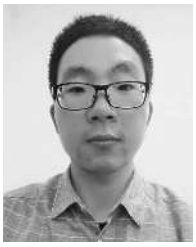

GUO XIAOJIE was born in Henan, China, in 1990. He received the B.S. degree from the Automation Department, Harbin Engineering University, Harbin, in 2014, where he is currently pursuing the Ph.D. degree.

His research interests include multi-phase motor control, coordinated fault-tolerant control, and ship electric propulsion system design.

ZHANG LANYONG (M'16) received the Ph.D. degree in theory and control engineering in 2011. His current research interests include the fast transient analysis and modeling of field-excited multiconductor networks, power-line carrier propagation, electromagnetic field interference from overhead multiconductor lines, and electromagnetic interaction with advanced composite materials. In 2009, he received the Excellent Graduate Award from the Harbin Engineering University.

He is currently a Master's Supervisor with the Harbin Engineering University. His main research interests are electromagnetic compatibility prediction and measurement, and stochastic signal processing.